Salt spray resistance of superhydrophobic waterborne polyurethane/carbon dots nanocomposites

O. S . Bankole-Ojo[1]*, F. O. Oyedeji[2], K.V.S.N. Raju[3], N. Ramanuj[3]

[1]*Industrial Chemistry Programme, Department of Physical and Earth Sciences, College of Pure and Applied Sciences, Crawford University, Ogun State, Nigeria.*
[2]*Department of Chemistry, University of Ibadan, Ibadan, Oyo State, Nigeria*
[3]*Polymer and Functional Polymers Division, Indian Institute of Chemical Technology, Hyderabad, Telangana, India*
olufunshobankole@crawforduniversity.edu.ng

Abstract

In this study, novel carbon quantum dots (cqds) has been synthesized through the thermal decomposition of the aqueous extract of Phoenix dactylifera fruit pulp. Silane functionalized carbon quantum dots (Scqds) were prepared through the attachment of silane derivatives from tridecafluorooctyltriethoxysilane to the surface of the cqds. Results obtained from FTIR spectroscopy, DLS and TGA studies reveal that silane compounds adhered to the cqds to give Scqds. Silane modification of the cqds changed the wettability from hydrophilicity to hydrophobicity from contact angle measurements. WPU/cqds and WPU/Scqds showed excellent thermal stability from TGA and DTA and exhibited hydrophilicity and superhydrophobicity respectively. Steel substrates coated with WPU/Scqds exhibited superior anti-corrosion properties when compared with steel substrates coated with WPU/cqds. Less than 5% corroded area was obtained for steel substrates coated with WPU/Scqds 0.2% and WPU/Scqds 0.25% after 96 hours when subjected to salt spray test. The intrinsic hydrophobicity of WPU/Scqds appear beneficial to inhibit the permeation of corrosive medium and consequently slow down the corrosion rate.

1. Introduction

Metal corrosion is an irreversible reaction of a metal with its environment which results in consumption of the metal or in dissolution of the metal into the environment. The global cost of corrosion in 2017 was estimated to be US$2.5 trillion, which is equivalent to roughly 3.4 percent of the global Gross Domestic Product (GDP). A common, efficient and cost effective method applied in tackling corrosion involves the application of anticorrosive coatings, such as epoxy [1-3], polyester, alkyd resin [4,5], or polyurethane coatings [6-8].

Polyurethane (PU) is widely used as an anti-corrosion coating due to its good adhesion to a wide range of substrates and resistance to corrosion [9]. Traditional PU coating techniques involved the use of volatile organic polymerization compounds during the manufacturing and application processes [10-12]. Volatile organic polymerization compounds have been identified as a serious environmental and public safety threat [13]. Two component waterborne polyurethane coatings have gained tremendous interest as alternative anti-corrosion coatings. Several studies have been performed using various resins to highlight the advantage of using two component waterborne polyurethanes [14-22].

Waterborne polyurethanes have been reinforced using boron nitride nanosheets. It was discovered that the corrosion resistance and anti-friction properties improved slightly. However, significant

improvement was observed with the hydroxyl functionalization of the boron nitride nanosheets [23]. Silane functionalized graphene oxide have been synthesized and incorporated into waterborne polyurethanes. The electrochemical impedance spectroscopy studies showed that manifested that the WPU coating exhibited good anti-corrosion properties [24]. WPU containing sulfonated graphene/zinc phosphate composites have been produced for anti-corrosion applications. It was observed that the anti-corrosion properties of the composites improved as the percentage of the filler increased [25].

WPU composites containing polyether amine functionalized graphene oxide was produced via in situ polymerization [26]. The study showed that the properties of WPU composites, such as hydrophobicity, thermal stability, mechanical and anti-corrosion properties were significantly improved due to the presence of the amine functionalized graphene oxide. WPU coating containing polyhedral silsesquioxane functionalized graphene oxide exhibited superior anti-corrosion properties compared to bare WPU [27]. Multifunctional polyhedral oligomeric silsesquioxane functionalized graphene oxide incorporated into WPU has been proven to give superior corrosion protection performance as observed by electrochemical impedance spectroscopy and potentiodynamic polarization [28].

Carbon quantum dots (cqds) are quasi-spherical nanomaterials below 10 nm in size [29]. They are composed of amorphous to crystalline sections with sp^2-graphitic carbon and sp^3-hybridized carbon framework [30]. Cqds have attracted significant attraction in recent years because of their photoluminescence, large surface to volume ratio, sensitivity to specific compounds or materials and ease of functionalization [31]. These properties have been utilized for applications such as biosensing, catalysis, bioimaging, wound healing, antibacterial and anti-corrosion applications [32]. In this study, cqds with average particle size of 9 nm were successfully synthesized from *Phoenix Dactylifera* fruit pulp through a one-step reflux method. The cqds were silane functionalized to produce hydrophobic cqds (Scqds). The bare and silane modified cqds were separately incorporated into WPU. The WPU/cqds and WPU/Scqds nanocomposites were spin coated on mild stainless steel plates and the respective salt spray resistance of the coated surfaces was evaluated.

2.   Materials and methods

2.1 Materials

Double distilled water with mean pH value of 6.6±0.3 and mean conductivity of 0.2±0.08 µScm^{-1} at an ambient temperature of 27°C was used for all experiments. Analytical grade absolute ethanol was purchased from SD fine chemicals, Mumbai. Dynasylan F8261 (tridecafluorooctyltriethoxysilane) was purchased from Evonik Co., Waterborne polyurethane (NeoRez R-9679) with a solid content of 37% was purchased from DSM (Netherlands). Q235 Steel substrates with a dimension of 100 mm × 50 mm × 1 mm was abraded using sandpaper. The steel substrates were washed with absolute ethanol and deionized water prior to coating application.

2.2 Plant collection and identification

The *Phoenix dactylifera* fruits were purchased between August and November from the Polimeraas:The Farmer's House, Nacharam - Mallapur Rd, MBD Complex, HMT Nagar, Tarnaka, Hyderabad, Telangana 500007, India, (17°42'29.9"N, 78°.54'61.6"E). Taxonomic identification was done by Dr. G. Baskar Rajan, the head of the botanical garden. Date fruits were washed with double distilled water and cut open to remove the seeds. The date fruits were thinly sliced and stored at -20°C in a freezer.

2.3 Synthesis of carbon quantum dots

Typically, 10g of the pulverized date fruit was dissolved into 150ml of deionized water in a round bottom flask placed in a silicone oil bath. The solution was refluxed under continuous stirring. The reaction was continued for 12 hours until the color of the solution turned dark brown. The solution was dialyzed against 1 litre deionized water using dialysis membrane (MWCO of 1000 Da). During the dialysis process, the water was changed every two hours. The aqueous solution of carbon quantum dots (cqds) was stored at 4°C for further experimentation.

2.4 Silane modification of cqds

Tridecaflurooctyltriethoxysilane (FAS 8261), a bifunctional fluoroalkylsilane that possesses hydrolysable ethoxysilyl groups and a fluoroalkyl chain was used as the surface coupling agent. 50-250 mg of lyophilized carbon quantum dots were dispersed in ethanol 5g of ethanol solution and sonicated, then 5mg of tridecaflurooctyltriethoxysilane was added to give varied fluoroalkylsilane to cqds ratios of 0.1:1, 0.05:1, 0.03:1, 0.025:1, 0.02:1 with respect to the fluoroakylsilane labelled as Scqds 0.1, Scqds 0.05:1, S:cqds0.03:1, Scqds0.025:1, Scqds0.02:1. The solution was stirred for 4 hours under ambient conditions to promote the attachment of the fluoroalkylsilane to the carbon quantum dots. The dried fluoroalkylsilane functionalized carbon quantum dots were lyophilized at -80°C for 12 hours.

2.5 Preparation of WPU/cqds and WPU/Scqds nanocomposites

Various dosages (9.25mg, 18.5mg, 27.75mg, 37mg, 46.25mg) of cqds and Scqds were dispersed in 8.5 mL of deionized water and ultrasonically dispersed for 1 h, and then 10 g of WPU was added and stirred vigorously for 1 h with a magnetic stirrer to give corresponding percentages of 0.05%, 0.1%, 0.15%, 0.2% and 0.25%. The WPU composite coatings reinforced by cqds and S:cqds 0.1:1 were named WPU/cqds and WPU/Scqds respectively.

2.6 Spin Coating on to glass and steel substrates

75 mm by 25 mm glass slides were thoroughly cleaned by sonicating in 70% nitric acid for 10 minutes and thereafter rinsed with water and acetone. Q235 steel substrates with a dimension 100 mm by 50 mm by 1mm steel substrates were abraded using sand-papers. Then these samples were washed with deionized water and acetone prior to application of coating.

Thin films of the appropriate solutions were deposited on the substrates using an Apex spinNXG-P2 spin coater at an ambient temperature of 24°C. An initial acceleration of 500 rpm and a maximum speed of 6000 rpm for a total time of 60 seconds were maintained for all samples. Static dispense coating was used initially and followed up by dynamic dispense coating twice at 6000 rpm to achieve a thin uniform triple layer. The coated substrates were air-dried for 3 hours and transferred to a vacuum oven and where it was heated at 105 °C for 30 mins.

2.7 Characterization

Transmission electron micrographs were developed from a JEOL JEM-100CX transmission electron microscope to study the size and morphology of carbon quantum dots. Fourier Transform Infrared (FTIR) spectroscopy study were performed using Thermo Nicolet Nexus 670 spectrometer. The groups attached to the cqds were investigated by FTIR spectroscopy using the KBr disc method at an ambient temperature of 25 °C. UV-vis absorption spectra were obtained using a Shimadzu 220V (E) UV-Vis spectrophotometer. Measurements were performed at an ambient temperature of 25 °C. Fluorescence

spectroscopy was performed with a Horiba Fluoromax 4 spectrophotometer at different excitation wavelengths. Measurements were performed at an ambient temperature of 25 °C.
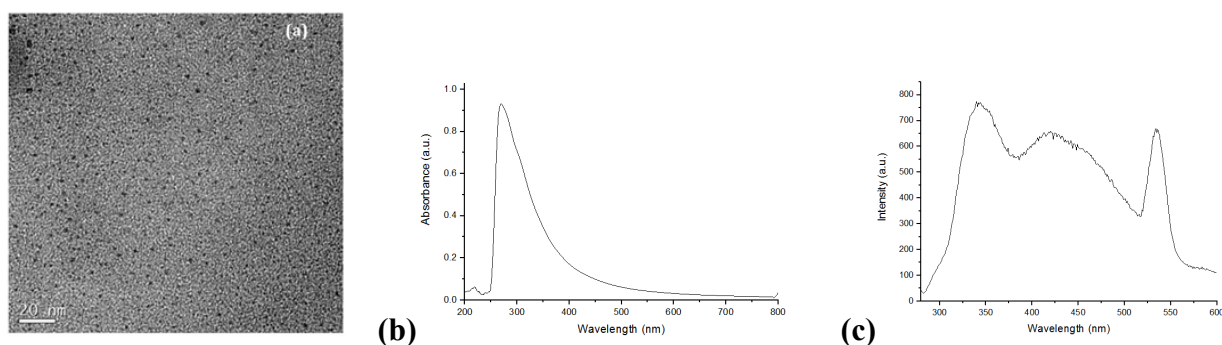
For the thermogravimetric analysis (TGA), 20 mg of the sample was placed in a TGA cell (Perkin-Elmer TG/DTA, Diamond) and heated to 900°C at a heating rate of 20 °C/ min in an atmosphere of N_2 gas. X-ray Diffraction (XRD) measurement of the polymers were performed in a θ-θ mode up to 80 degrees (2θ) by a Siemens D- 5000 X-ray diffractometer with Cu Kα radiation (λ = 0.154 nm) and a measurement temperature of 25°C. Water to air contact angles were measured using G10 (KRUSS) which uses the sessile drop technique was used for the measurement at a temperature of 24°C.

The salt spray test was carried out on coated Q235 plates (50 mm × 100 mm) with a 5 wt % NaCl solution at 100% relative humidity at 35 °C according to ASTM B117-03. The % corroded/slightly corroded area was determined using the ImageJ analysis software as performed by Chen et al. (2012).

3. Results and Discussion

3.1 Characterization of cqds

The morphology and microstructure of the cqds were investigated using TEM (Fig 1a). TEM analysis showed cqds with with an average size of 7 nm. The absorption spectrum (Fig 1b) showed a wavelength of maximum absorption at 273 nm which could be associated with π-π* transition. The fluorescence emission spectrum of the cqds at an excitation wavelength of 270 nm is illustrated in Fig. 1c with visible peaks at 330 nm, 420 nm and 540 nm.
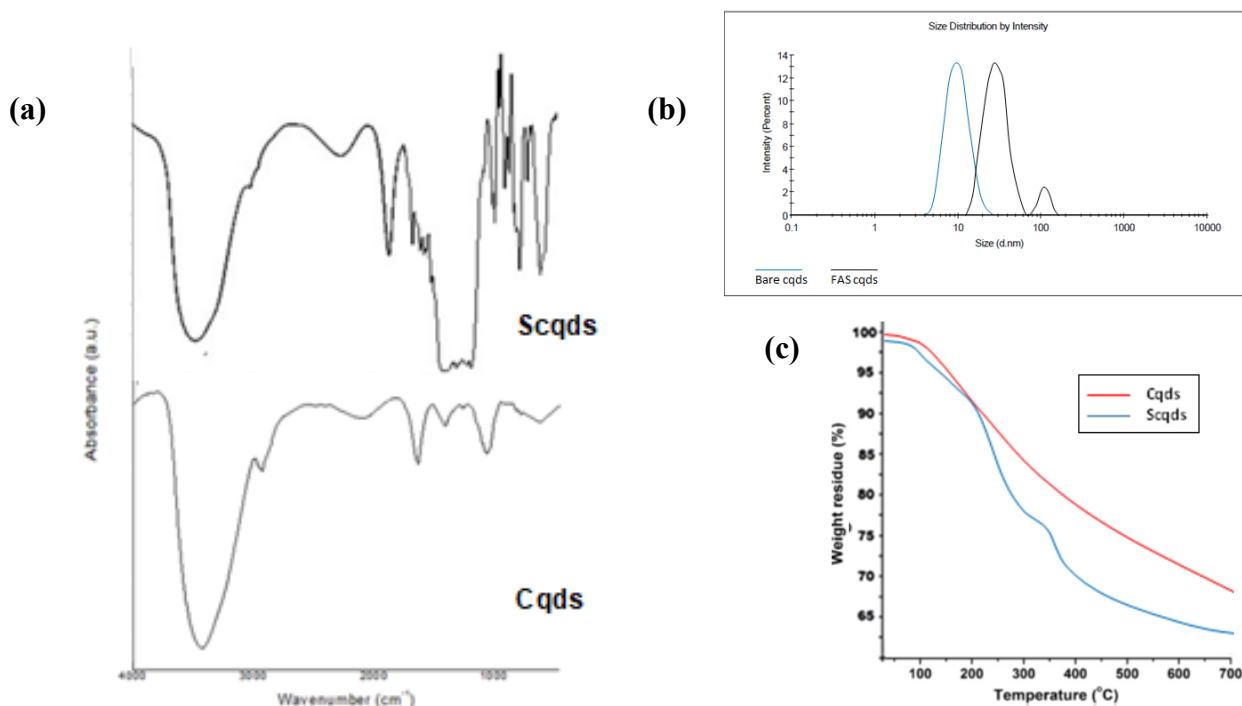

Fig 1. (a) TEM image of cqds (b) UV/vis spectrum of cqds (c) Photoluminescence spectrum of cqds

3.2 Characterization of cqds and Scqds

An FTIR spectra of cqds and Scqds (Fig 2a) was utilized to investigate the silane modification of the cqds. The FTIR spectrum of cqds shows a broad peak at 3645 cm⁻¹ that could be attributed to C–OH stretching vibrations. The characteristic peaks observed at 1647, 2975, and 1049 cm⁻¹ corresponds to –C=C– (aromatic), C H (aromatic) and C–O functional groups respectively. This is similar to results obtained from previous studies [33-35]. For the silane modified cqds, the frequency band at 3650 cm⁻¹ is related to O-H stretching from OH groups. The band at 2980cm⁻¹ can be attributed to C-H stretching. The intense band at 1617 cm⁻¹ is related to C=C stretching. Intense absorptions recorded at 1453 cm⁻¹, 1392 cm⁻¹ and 1368 cm⁻¹ are most likely due to the presence of CH_2 and CH_3 groups. The frequency bands at 1220 – 1130 cm⁻¹ can be attributed to C-F_2. The peaks at 870 cm⁻¹, 805 cm⁻¹, 775 cm⁻¹ and 705 cm⁻¹ can be related to C-F_3 bonds. The band at 564cm⁻¹ can be attributed to O-Sn-O. DLS analysis was carried out to highlight the change in hydrodynamic size due to silane modification of cqds. Average hydrodynamic size of 14 nm was obtained for cqds while for Scqds an average hydrodynamic size of 61 nm was obtained. To further understand the silane attachment,

thermogravimetric analysis (TGA) was performed on cqds and Scqds (Fig. 2c.) For the cqds, there are two important steps of weight loss at 140ºC and 305ºC which may be due to the loss of water molecules and oxygen bearing groups associated with the surface of the cqds. The Scqds exhibited multiple weight losses. The initial loss at 120ºC is assigned to water molecule and other oxygen bearing groups as explained above. Further reduction in the weight at 320ºC and 490ºC are due to the loss of the fluoralkylsilane groups and other functional groups.
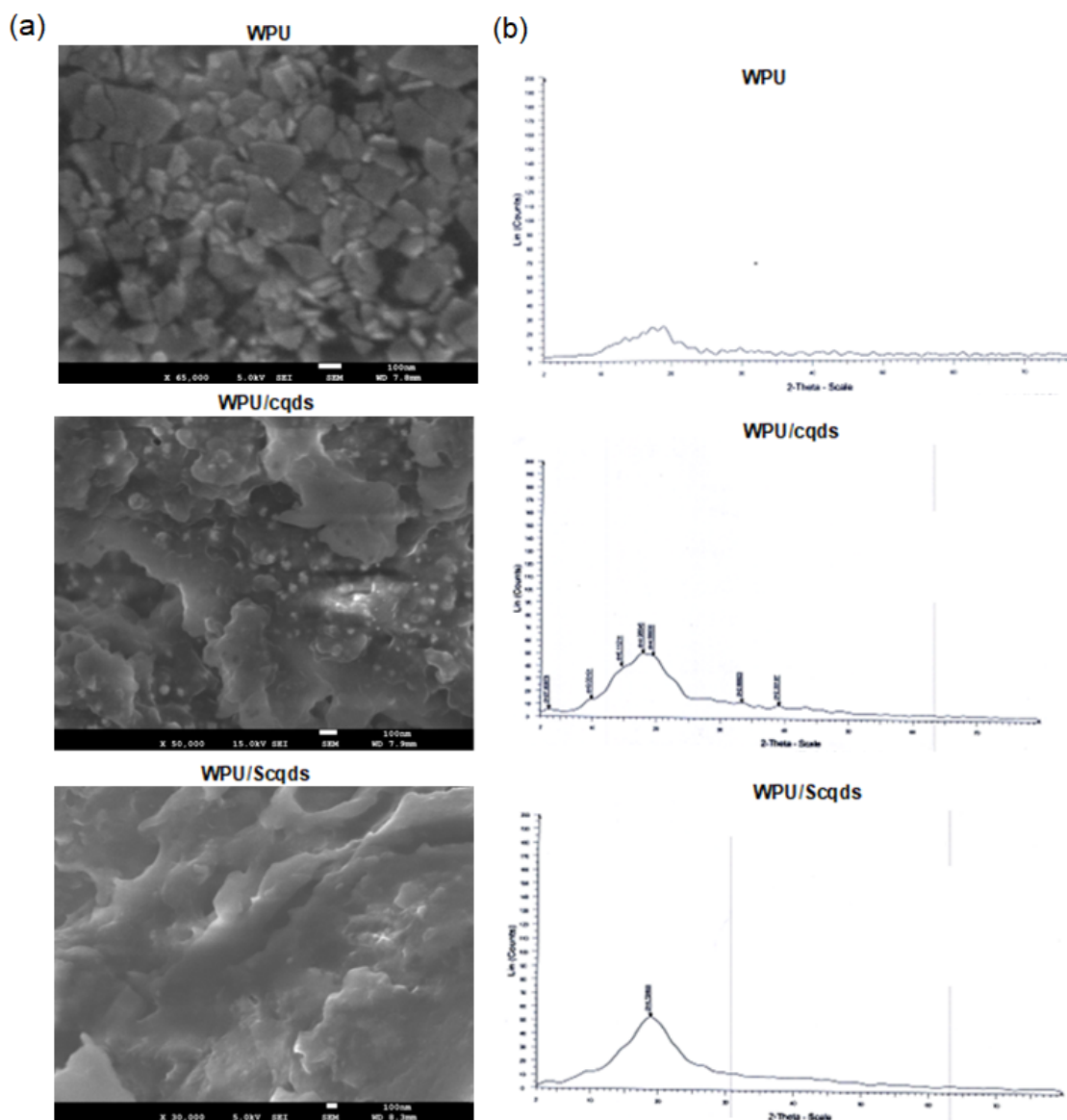

Fig 2. (a) FTIR spectra of cqds and Scqds (b) DLS image of cqds and Scqds (c) TGA of cqds and Scqds.

3.3 Characterization of WPU, WPU/cqds and WPU/Scqds

To understand the dispersion and interfacial interaction of cqds and Scqds in WPU coatings, the surface and cross-sectional morphologies of coating specimens were studied through FESEM analysis (Fig 3a). The pure WPU coating showed polymer particles locked into each other with visible spaces and a high degree of disorderliness. The WPU/cqds coating showed less distinct particles held together to form a much smoother surface. The WPU/Scqds coating produced a much smoother surface. XRD studies showed strong 002 diffraction peak for the WPU at $2\theta=24º$. The diffraction peak of WPU/cqds produced a diffraction peak with higher intensity $2\theta=24º$. The diffraction peak of WPU/Scqds produced a diffraction peak with similar intensity $2\theta=24º$. The reason for increment in the intensity of the diffraction peaks is due to the strong interactions in between the polar functional groups of the cqds and polymer matrix (Fig 3b).

Thermogravimetric (TGA) analysis shown in Fig. 4a was performed on the WPU and WPU composites to study their thermal behavior. DTA curves shown in Fig. 4b shows a degradation pattern characterized by a single step process with maximum weight loss around 300–450ºC. The initial weight loss started in the temperature range of 100–150ºC. The initial degradation corresponds with the loss of volatiles and moisture. Further degradation at 300–450ºC shows that the degradation temperature
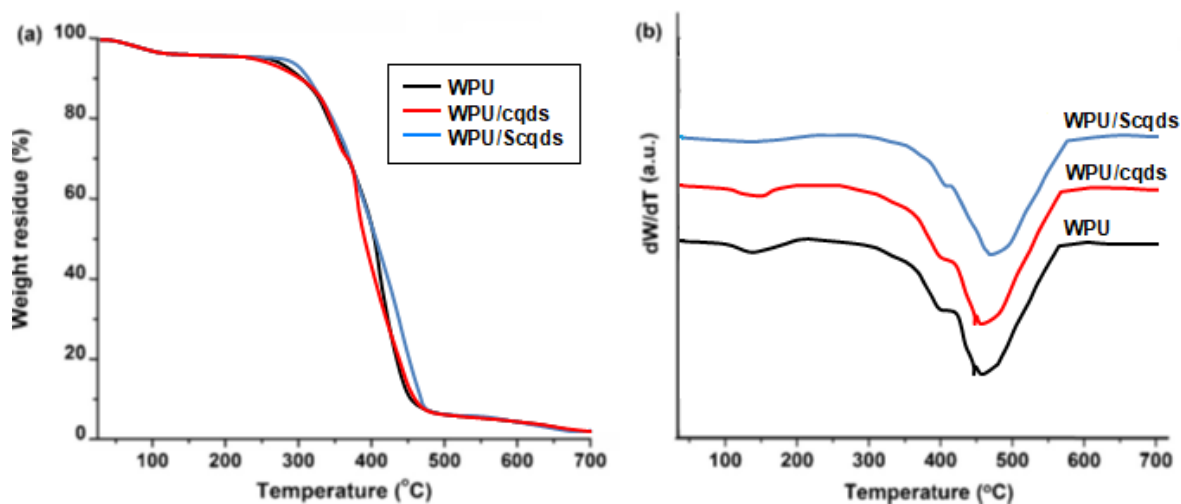
increases as one moves from WPU to WPU/cqds and WPU/Scqds. The good thermal stability of the WPU nanocomposites is due to the existence of primary and secondary interactions imparted by the cqds with the polymer chain resulting in high cross link density. The superior property of the WPU/Scqds is as a result of the restriction on the mobility of the polymeric chains resulting in improved thermal stability of the WPU/Scqds nanocomposite. Thus, the thermal stability of WPUs can be enhanced by adding cqds or Scqds.
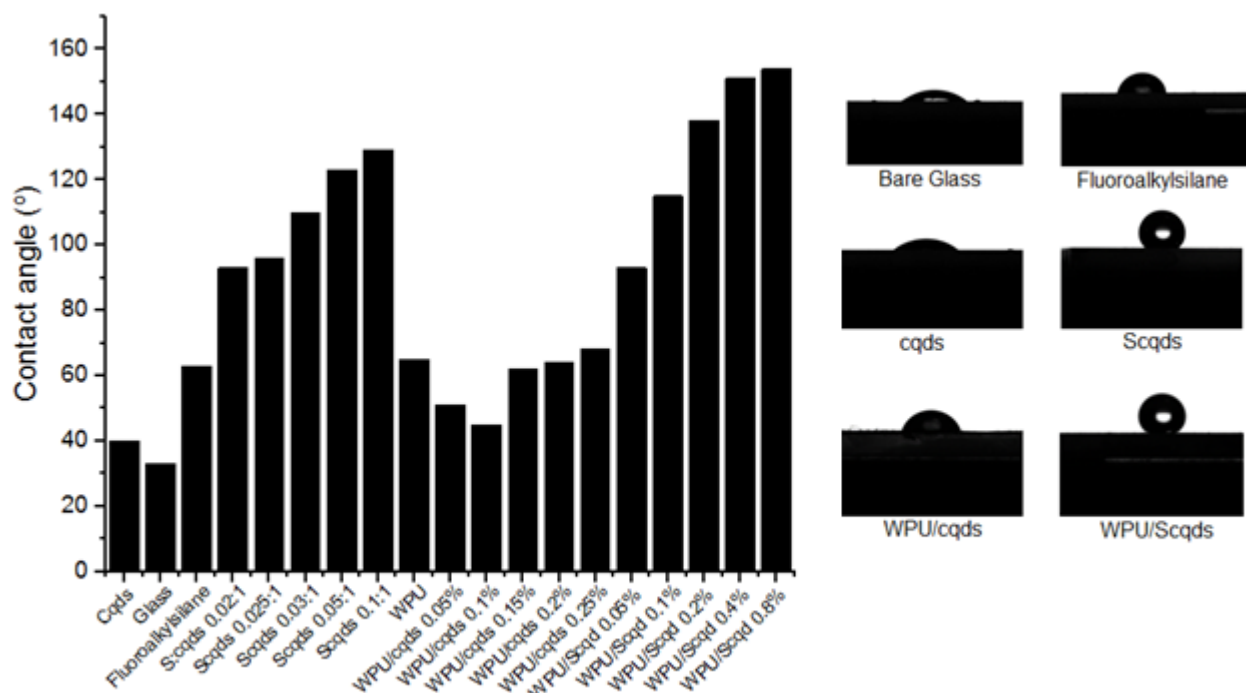

Fig 3. (a) FESEM images of WPU, WPU/cqds and WPU/Scqds (b) XRD patterns of WPU, WPU/cqds and WPU/Scqds.

Contact angle measurements were performed to assess the relative wettability of the coated and un-coated surfaces as seen in Fig. 5. Bare glass, cqds on glass and pure WPU exhibited hydrophilicity with static water contact angles less than 80°. Silane modification improved the non-wetting property of the coatings significantly. Static water contact angle values above 90° were obtained for the glass substrates coated with Scqds. The WPU/cqds coatings exhibited hydrophilicity as a result of the abundance of hydroxyl groups on the surface of the coatings. The static water contact angles obtained for WPU/cqds coatings were higher than that obtained for cqds but remained within the hydrophilic range. The

WPU/Scqds coated surfaces produced hydrophilic surfaces and attained superhydrophobicity at WPU/Scqds 0.4% and WPU/Scqds 0.8%. The WPU/Scqds coated surfaces produced static water contact angles above that of the Scqds coated surfaces. This is as a result of the much rougher surfaces of the WPU/Scqds coatings which produced the superhydrophobic surfaces.
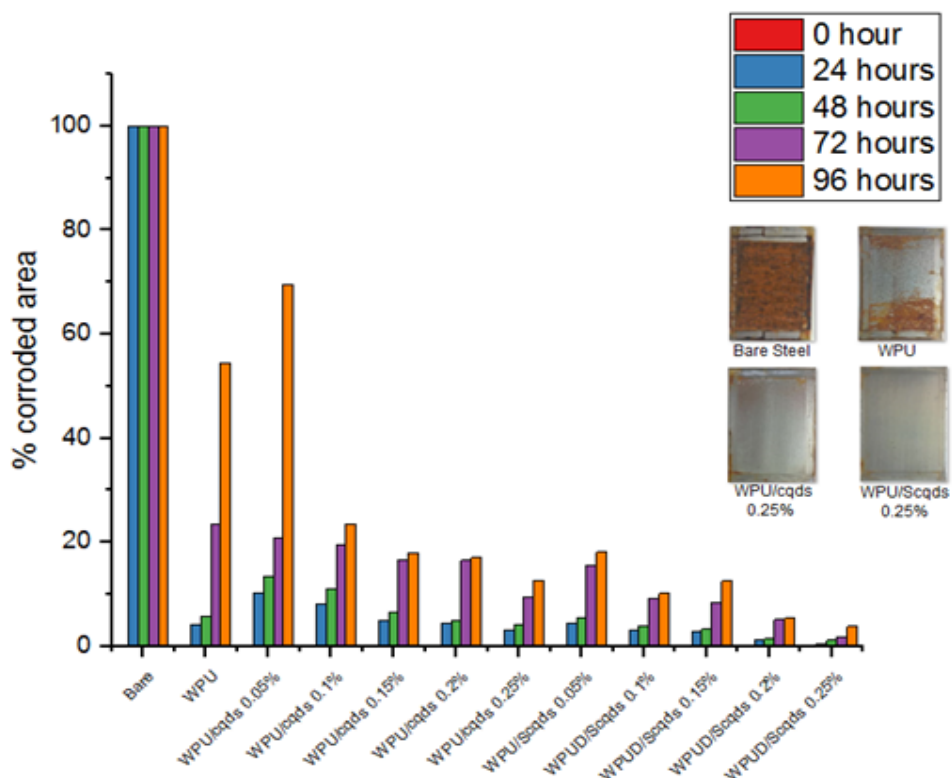

Fig 4. (a) TGA thermograms (b) DTA curves of WPU, WPU/cqds and WPU/Scqds.

Fig. 5. Contact angles of cqds, Scqds, WPU/cqds and WPU/Scqds

Spray resistance of WPU and WPU composites on steel substrates was estimated and the results are presented in Fig. 6. Bare steel substrates were completely corroded after 24 hours. Steel substrates coated with WPU/cqds coatings at concentration lower than 0.05% showed lesser salt spray resistance with more than 60% corroded area after 96 hours than WPU coatings with less than 60% corroded area. This is as a result of inadequate cqds to strengthen the mechanical properties of the composite and the presence of free hydroxyl group due to the surface carbon dots with hydroxyl groups. Steel substrates

coated with WPU/cqds coatings at concentration higher than 0.05% showed greater salt spray resistance with less than 30% corroded area after 96 hours than WPU coatings as a result of stronger mechanical properties of the coating serve as a better corrosion inhibitor. The WPU/Scqds coatings showed superior salt-resistance when compared to WPU/cqds. The WPU/Scqds coated surfaces generally showed less than 20% corroded area after 96 hours. WPU/Scqds 0.25% only exhibited small traces of corrosion after 96 hours with less than 5% corroded area. The good mechanical properties of the coating, superhydrophobic nature of the surface and the strong attachment of the WPU/Scqds 0.25% coatings to the steel substrates serve as important factors that ensure the formation of a good barrier which serves as an excellent corrosion inhibitor. The results highlights the good anti-corrosion potential of Scqds incorporated into waterborne polyurethanes for coating applications.

Fig. 6. Percentage corroded area of steel plates coated with WPU/cqds and WPU/Scqds.

Conclusion
Cqds with sizes less than 9 nm were synthesized from *Phoenix dactylifera* (date) fruit pulp The cqds were silane modified and FTIR analysis confirmed the silane modification. Cqds and Scqds were incorporated into waterborne polyurethane and coated on glass and steel surfaces. Contact angle measurements indicated that the WPU/cqds coatings produced hydrophilic surfaces as a result of the abundance of hydroxyl groups on the surface of the coatings. WPU/Scqds coatings produced superhydrophobic surfaces as a result of the silane groups acting on the surface. Steel substrates coated with WPU/Scqds exhibited superior anti-corrosion properties when compared with steel substrates coated with WPU/cqds. Less than 20% corroded area was observed for steel substrates coated with WPU/Scqds after 96 hours and specifically, less than 5% corroded area was observed for steel substrates coated with WPU/Scqds 0.2% after 96 hours when subjected to salt spray test. This highlights the strong potential of the WPU/Scqds coatings for anti-corrosion applications.

Conflicts of Interest: The authors declare that they have no conflict of interest.

References

[1] J. Ding, H. Zhao, & H. Yu, Bio-inspired Multifunctional Graphene–Epoxy Anticorrosion Coatings by Low-Defect Engineered Graphene. *ACS nano*, 16(1) (2022) 710-720. https://doi.org/10.1021/acsnano.1c08228

[2] S. R. Nayak, K. N. S. Mohana, M. B. Hegde, K. Rajitha, A. M. Madhusudhana, & S.R. Naik, Functionalized multi-walled carbon nanotube/polyindole incorporated epoxy: An effective anti-corrosion coating material for mild steel. *Journal of Alloys and Compounds*, 856 (2021) 158057. https://doi.org/10.1016/j.jallcom.2020.158057

[3] A. Diraki, & S. Omanovic, Smart PANI/epoxy anti-corrosive coating for protection of carbon steel in sea water. Progress in Organic Coatings, 168 (2022) 106835. https://doi.org/10.1016/j.porgcoat.2022.106835

[4] P. Das, N. Sharma, A. Puzari, D.K. Kakati, N. Devi, Synthesis and characterization of neem (Azadirachta indica) seed oil-based alkyd resins for efficient anticorrosive coating application. *Polymer Bulletin,* 78(1) (2021) 457-479. https://doi.org/10.1007/s00289-02003120-8

[5] H. Tong, X. Liu, Y. Liu, H. Zhang & X. Li, Polyaniline modified attapulgite incorporated in alkyd paint for carbon steel corrosion inhibition. *Corrosion Engineering, Science and Technology*, *56*(7) (2021) 618-625. https://doi.org/10.1080/1478422X.2021.1931646

[6] H. Wang, J. Xu, X. Du, Z. Du, X. Cheng, & H. Wang, A self-healing polyurethane based composite coating with high strength and anti-corrosion properties for metal protection. *Composites Part B: Engineering*, 225 (2021) 109273. https://doi.org/10.1016/j.compositesb.2021.109273

[7] Y. Feng, Y. Cui, M. Zhang, M. Li, & H. Li, Preparation of Tung Oil-Loaded PU/PANI Microcapsules and Synergetic Anti-Corrosion Properties of Self-Healing Epoxy Coatings. *Macromolecular Materials and Engineering*, 306(2) (2021) 2000581. https://doi.org/10.1002/mame.202000581

[8] M. Faccini, L. Bautista, L. Soldi, A. M. Escobar, M. Altavilla, M. Calvet & E. Domínguez, Environmentally friendly anticorrosive polymeric coatings. Applied Sciences, 11(8) (2021). 3446. https://doi.org/10.3390/app11083446

[9] M. Salzano de Luna, Recent Trends in Waterborne and Bio-Based Polyurethane Coatings for Corrosion Protection. *Advanced Materials Interfaces,* (2022) 2101775. https://doi.org/10.1002/admi.202101775

[10] R. Huang, X. Du, H. Wang, X. Cheng, & Z. Du, Highly stretchable polyurethane coating based on functionalized cerium oxide nanoparticles for anti-corrosive/UV protection. *Journal of Applied Polymer Science*, 139(15) (2022) 51927. https://doi.org/10.1002/app.51927

[11] G. Cai, S. Xiao, C. Deng, D. Jiang, X. Zhang, & Z. Dong, CeO_2 grafted carbon nanotube via polydopamine wrapping to enhance corrosion barrier of polyurethane coating. *Corrosion Science*, *178* (2021) 109014. https://doi.org/10.1016/j.corsci.2020.109014

[12] H. Tan, Y. Guo, J. Wang, D. Wang, & Y. Cui, The effect of additive particle size on the anti-corrosion behavior of PU coating. *Anti-Corrosion Methods and Materials.* (2021). https://doi.org/10.1108/ACMM-08-2020-2359

[13] K. Kim, H. M. Shin, L. Wong, T.M. Young, & D. H. Bennett, Evaluating couch polyurethane foam for a potential passive sampler of semivolatile organic compounds. *Chemosphere* (2021) 129349. https://doi.org/10.1016/j.chemosphere.2020.129349

[14] L. D. Agnol, F. T. G Dias, H. L. Ornaghi Jr, M. Sangermano, O. Bianchi, UV curable waterborne polyurethane coatings: A state-of-the-art and recent advances review. *Progress in Organic Coatings*, *154* (2021) 106156. https://doi.org/10.1016/j.porgcoat.2021.106156

[15] A. M. Palve, K. Mensah-Darkwa, F. M. D. Souza, R. K. Gupta, Applications of Cationic Waterborne Polyurethanes. In *Sustainable Production and Applications of Waterborne Polyurethanes* (2021) 47-65. Springer, Cham. https://doi.org/10.1007/978-3-030-72869-4_5

[16] A. Santamaria-Echart, I. Fernandes, F. Barreiro, M. A. Corcuera, & A. Eceiza, Advances in waterborne polyurethane and polyurethane-urea dispersions and their eco-friendly derivatives: A review. *Polymers*, *13*(3) (2021) 409. https://doi.org/10.3390/polym13030409

[17] Y. Qian, F. Dong, L. Guo, X. Xu, & H. Liu, Two-component waterbornepolyurethane modified with terpene derivative-based polysiloxane for coatings via a thiol-eneclick reaction. Industrial Crops and Products, 171 (2021) 113903.https://doi.org/10.1016/j.indcrop.2021.113903

[18] M. Ramesh, L. Rajeshkumar, D. Balaji, M. Priyadharshini, Properties and Characterization Techniques for Waterborne Polyurethanes. In *Sustainable Production and Applications of Waterborne Polyurethanes* (2021) 109-123.doi.org/10.1007/978-3-030-72869-4_6

[19] X. Yin, H. Pang, Y. Luo, & B. Zhang, Eco-friendly functional two-component flame retardant waterborne polyurethane coatings: a review. Polymer Chemistry. (2021) https://doi.org/10.1039/D1PY00920F

[20] M. Dai, Y. Zhai, & Y. Zhang, A green approach to preparing hydrophobic, electrically conductive textiles based on waterborne polyurethane for electromagnetic interference shielding with low reflectivity. Chemical Engineering Journal, 421 (2021) 127749. https://doi.org/10.1016/j.cej.2020.127749

[21] X. Yin, & Y. Luo, Green fluorescent waterborne polyurethane polyols. Colloid and Polymer Science, 299(5) (2021) 845-853. https://doi.org/10.1007/s00396-021-04807-8

[22] P. Yi, J. Mo, R. Liu, B. Fan, K. Xiao, J. Gao, & H. Zhou, Study on Corrosion Behavior of Waterborne Polyurethane Coating with High Thermal Conductivity. *Applied Sciences*, *12*(4) (2022). https://doi.org/10.3390/app12042021

[23] H. Liu, W. Hao, & Y. Qin, In situ preparation and properties of waterbornepolyurethane/edge-isocyanated hexagonal boron nitride composite dispersions. *J. Coatings Tech. and Research*, *18*(1) (2021).https://doi.org/10.1007/s11998-020-00385-6

[24] M. Salzano de Luna, Recent Trends in Waterborne and Bio-Based Polyurethane Coatings for Corrosion Protection. *Advanced Materials Interfaces*, 9(11) (2022) 2101775. https://doi.org/10.1002/admi.202101775

[25] J. Zhang, J. Wang, S. Wen, S. Li, Y. Chen, J. Wang, & Y. Mao, Waterborne Polyurea Coatings Filled with Sulfonated Graphene Improved Anti-CorrosionPerformance. *Coatings*, *11*(2) (2021) 251. https://doi.org/10.3390/coatings11020251

[26] X. Sheng, S. Li, H. Huang, Y. Zhao, Y. Chen, L. Zhang & D. Xie, Anticorrosive and UV-blocking waterborne polyurethane composite coating containing novel two-dimensional Ti_3C_2 MXene nanosheets. Journal of Materials Science, 56(6) (2021) 4212-4224. https://doi.org/10.1007/s10853-020-05525-2

[27] F. Zhang, S. Wang, W. Liu, H. Shi, L. Liang, C. Liu, & J. Zeng, Design on the corrosion protection of eco-friendly and multifunctional polyhedral oligomeric silsesquioxane functionalized graphene oxide reinforced waterborne polyurethane. Colloids and Surfaces A: Physicochemical and Engineering Aspects, 640 (2022) 127718. https://doi.org/10.1016/j.colsurfa.2021.127718

[28] R. Shen, M. Long, C. Lei, L. Dong, G.Yu, & J. Tang, Anticorrosive waterborne polyurethane coatings derived from castor oil and renewable diols. *Chemical Engineering Journal*, *433* (2022) 134470. https://doi.org/10.1016/j.cej.2021.134470

[29] R. M. El-Shabasy, M. Farouk Elsadek, B. Mohamed Ahmed, M. Fawzy Farahat, K. N. Mosleh, M. M. Taher, Recent developments in carbon quantum dots: properties, fabrication techniques and bio-applications. *Processes*, 9(2) (2021) 388. https://doi.org/10.3390/pr9020388

[30] M. R. Silva, M. F. Alves, M. H. Fernandes, P. M. Vilarinho & P. Ferreira, Carbon Quantum Dot-Based UV-Protective Coatings. *Materials Proceedings*, 8(1) (2022) 106. https://doi.org/10.3390/materproc2022008106

[31] A. Hosseinpour, M. R. Abadchi, M. Mirzaee, F. A. Tabar & B. Ramezanzadeh, Recent advances and future perspectives for carbon nanostructures reinforced organic coating for anti-corrosion application. *Surfaces and Interfaces*, 23 (2021) 100994. https://doi.org/10.1016/j.surfin.2021.100994

[32] T. W. Quadri, L. O. Olasunkanmi, O. E. Fayemi, & E. E. Ebenso, Functionalized Carbon Allotropes as Corrosion Inhibitors. In *Functionalized Nanomaterials for Corrosion Mitigation: Synthesis, Characterization, and Applications*, (2022) 87-114. American Chemical Society. https://doi.org/10.1021/bk-2022-1418.ch004

[33] S. Borna, R. E. Sabzi, & S. Pirsa, Synthesis of carbon quantum dots from apple juice and graphite: investigation of fluorescence and structural properties and use as an electrochemical sensor for measuring Letrozole. *Journal of Materials Science: Materials in Electronics*, *32*(8) (2021) 10866-10879. https://doi.org/10.1007/s10854-021-05745-5

[34] J. S. Boruah, K. Sankaranarayanan, & D. Chowdhury, Insight into carbon quantum dot vesicles interactions: role of functional groups. *RSC advances*, *12*(7) (2022) 4382-4394. https://doi.org/10.1039/D1RA08809B

[35] O. G. Rojas-Valencia, M. Regules-Carrasco, J. Hernández-Fuentes, C. M. Reza-San Germán, M. Estrada-Flores & E. Villagarcía-Chávez, Synthesis of blue emissive carbon quantum dots from Hibiscus Sabdariffa flower: Surface functionalization analysis by FT-IR spectroscopy. *Materialia*, *19* (2021) 101182. https://doi.org/10.1016/j.mtla.2021.101182

(2022) ; http://www.jmaterenvironsci.com